Experimental Thermal and Fluid Science, Volume 120, January 2021, Article number 110247
DOI:10.1016/j.expthermflusci.2020.110247

Experimental study of a single elongated bubble in liquid in under 10-degree upwardly inclined pipes

Aniefiok Livinus[1], Patrick G. Verdin[2],

1. Chemical and Petroleum Engineering Department, University of Uyo, P.M.B 1017, Uyo, Akwa Ibom State, Nigeria.
2. Energy & Power, School of Water, Energy and Environment, Cranfield University, MK43 0AL, UK.

Abstract

Two phase flow is of great interest in chemical and petroleum industries, and multiphase pipe flow models with closure relationships require experimental data for their development and validation. However, only little experimental information is available for slightly upward inclined pipes. Experimental investigations of single elongated bubble in marginally upwardly inclined pipes less than 10^o have therefore been performed. Observations of the bubble drift velocity along the pipe has been highlighted. The drift velocity data presented here can contribute to improve knowledge of pipe inclination and viscosity dependency in drift velocity correlations. The new data on the bubble characteristics - shape, length, fraction and drift velocity may also provide useful information for the development and validation of numerical models. The measured drift velocity data have therefore been compared with some recently developed bubble velocity correlations.

Keywords: Long bubble, bubble characteristics, inclined pipe, slug flow models, drift flux models.

Nomenclature and Abbreviations

C_o, Co	Velocity distribution parameter in drift flux model, depends on the velocity profile in the liquid, and is approximately the ratio of the maximum to the mean velocity.	dimensionless
D	Pipe diameter	m
Eo	Eötvös Number; the ratio of the gravitational forces to the interfacial forces.	dimensionless
$\mathrm{N_{vis}}$	Viscosity number; the ratio of the viscous forces to the gravitational forces.	dimensionless
Fr	Froude Number; the ratio of the bubble inertia to the gravitational forces.	dimensionless
R	Buoyancy Reynolds number; the ratio of the gravitational forces to the viscous forces	dimensionless

Mo	Morton number, which primarily relates the viscous forces to surface tension forces.	dimensionless
fps	Frame per second	1/s
g	Acceleration due to gravity	m/s^2
ID	Internal diameter pipe	m
L/D	Ratio of pipe length to pipe diameter	dimensionless
Lb/D	Ratio of bubble length to pipe diameter	dimensionless
h/D	Liquid height Parameter	dimensionless
v_d	Drift velocity	m/s
v_m	Mixture velocity	m/s
U_B	Slug bubble velocity	m/s
V_N	Bubble front velocity	m/s
V_T	Bubble tail velocity	m/s
ρ	Mass density	kg/m^3
μ	Dynamic viscosity	kg/m-s
μ_l/μ_w	Viscosity ratio; as defined in this work, is the ratio of the dynamic viscosity of a liquid, μ_l, to the dynamic viscosity of water, μ_w, as a reference.	
σ	Surface tension	N/m
θ	Pipe inclination relative to horizontal	Degree
VOLgas	Estimated gas volume injection	m^3
LTT	Long Tapered Tail	
STT	Short Tapered Tail	
STwtB	Short Tapered with detached tiny Bubbles	

1.0 Introduction

Slug flow is one of the multiphase flow patterns present in the production and transportation of oil, which can create pressure fluctuations that can adversely affect oil facilities. It is characterized by a quasi-periodic alteration of long bubbles and liquid slugs. In vertical pipes, the elongated (Taylor) bubbles, as described by Fabre and Liné [1], rise with a round shaped front followed by a cylindrical main body

surrounded by an annular liquid film. When the pipe is other than vertical, the symmetry of the long bubble is lost; the transverse component of gravity causes the interface structure of long bubbles to change from an annular to a stratified flow pattern. Successful modelling of slug flow depends on the understanding of the motion of these long bubbles as they convey greater amount of the gas.

The investigation of the intermittent slug flow phenomena has been carried out systematically over the years in well-controlled experiments. For instance the works of Bendiksen [2], Fagundes et al. [3], Jeyachandra et al. [4], and Losi and Poesio [5], for the propagation of a single elongated bubble in stagnant or flowing liquid in pipes. The overall objective of these studies has been mostly to acquire data for improving the elongated bubble velocity in slug flow models. A summary of several experimental studies carried out on the characteristics of slug flow phenomena is presented in Table A-1. The findings generally reported by previous researchers, e.g. Bendiksen [2], Weber et al. [6], Hasan and Kabir [7], Shosho and Ryan [8], Van Hout et al. [9], Gockal et al. [10] and among others, show that the drift velocity increases with a decrease in oil viscosity, an increase in pipe diameter, and an increase in pipe inclination (with a maximum value at about 45°), and thereafter decreases. The propagation velocity is independent of length as long as the volume of the bubble corresponds to a cylinder with the tube radius and a length of 3 tube radii as reported by Zukoski [11]. Spedding and Nguyen [12] observed that the Froude number increases noticeably with the bubble volume at low tube inclination relative to the horizontal, and that beyond 2° of inclination relative to horizontal, the Froude number becomes nearly independent of the bubble size. Other findings reported by previous researchers, Bendiksen [2], Fagundes et al. [3], Woods and Hanratty [13], Grenier et al. [14], and among others, cover the bubble shape which depends on the mixture velocity, the fluid properties – viscosity and surface tension, and the pipe inclinations, but it's independent on the bubble length. On the aspect of the void fraction, the work of Fabre and Liné [1] reported that the void fraction in liquid slugs is hardly greater than 25% but its value may be as high as 90%. Measurements of the effects of pipe diameter, viscosity, and pipe inclinations on the void fraction of long bubbles in slug flows in horizontal and upward inclined pipes have also been reported in the works of Jeyachandra et al. [4], Gokcal et al. [10] and Woldesemayat and Ghajar [15].

The drift flux model is one of the major approaches used to analyse slug flow in pipelines. The slug bubble velocity which basically relies on the drift velocity, as shown in Equation (1) proposed by Nicklin [16], is one of the closure relationships in a slug flow model.

$$U_B = C_o v_m + v_d \tag{1}$$

where U_B is the summation of the maximum mixture velocity in the slug body and the drift velocity, C_o is the velocity distribution parameter, v_d is the bubble drift velocity and v_m is the mixture velocity. The distribution parameter, C_o, is a dimensionless coefficient that depends on the velocity profile in the liquid, and is approximately the ratio of the maximum to the mean velocity. Bendiksen [17] interpreted (1) as a general expression of U_B, being very close to the liquid velocity ahead of the bubble nose tip; $U_L(r_t) \approx C_o v_m$, plus a drift velocity, where r_t is the radial position of the tip. A comprehensive study on the modelling of two-phase slug flow can be found in Fabre and Liné [1], Taitel and Barnea [18] and

Bendiksen et al. [19]. It has been well-established that the long gas bubble's dynamics are influenced by the viscous, inertial, gravitational, and interfacial forces acting on it, see White and Beardmore [20]. Dimensional analysis has shown that at least three dimensionless pi -groups are sufficient to determine the bubble dynamics: the Froude number, which is the ratio of the bubble inertia to the gravitational forces; the Eötvös number, which is the ratio of the gravitational to interfacial forces; and the Morton number, which primarily relates the viscous forces to surface tension forces. The choice of the pi-groups is not unique; for example, the inverse viscosity number, a combination of Eötvös number and Morton number, can also be employed. Several researchers, Jeyachandra et al. [4], Viana et al. [21], Lizarraga-Garcia et al. [22], and Livinus et al. [23], have used different combinations of the dimensionless pi-groups and other set of independent dimensionless groups (e.g Reynolds number, Weber number and buoyancy Reynolds number) to represent the dynamics, especially the drift velocity, of the elongated bubbles found in a slug flow. The choice of the combination is such that the forces influencing the long bubble dynamics are well captured in a unique way. Mathematical definitions of some the widely used dimensionless groups are given as follows:

$$Fr_d = v_d/[(gD)(1 - {}^{\rho_g}/_{\rho_l})]^{1/2} \tag{2}$$

$$Eo = \frac{(\rho_l - \rho_g)gD^2}{\sigma} \tag{3}$$

$$Mo = \frac{g\mu^4}{\rho\sigma^3} \tag{4}$$

$$N_{vis} = \mu\left(gD^3(\rho_l - \rho_g)\rho_l\right)^{-0.5} \tag{5}$$

$$R = \frac{\left(D^3 g\left(\rho_l - \rho_g\right)\rho_l\right)^{0.5}}{\mu} \tag{6}$$

Some researchers, Gregory and Scott [24], Dukler and Hubbard [25], have proposed a zero drift velocity for slug flow models in horizontal or nearly horizontal pipes. However, theoretical works of Benjamin [26] and Weber [27], and the experimental works of Zukoski [11], Bendiksen [2], Weber et al. [6], have shown that drift velocity exists, even for horizontal flows. Unfortunately, most of the works have been directed towards low viscosity liquids, and only very few experiments have included high viscous liquids but have been performed in a short pipe length, for instance the works of Zukoski [11] and Weber et al. [6]. Zukoski [11] has already pointed out that the distance from the bubble front to the pipe exit for these short tubes was not enough to study the effect of viscous effects on the drift velocity along the pipe. Recent studies by Gokcal et al. [10], Jeyachandra et al. [4], Moreiras et al. [28], have included the study

of drift velocities for liquids with viscosities up to 1000 cP, with longer pipes covering a wide range of pipe inclinations but in a coarse interval of ±10°. In addition, the bubble velocity measurements have been reported only for a point along the pipe and there is no information of the bubble velocity behaviour along the pipe. For moderately inclined pipes (say, between 1° and 10°), the works of Cook and Behnia [29], Perron et al. [30], and Leonardo et al. [31], presented only the bubble velocity measurements for a point along the pipe in a liquid viscosity less than 22 cP. The study by Losi and Poesio [5] seems to be the only detailed study available in the open literature that included high viscosity liquid. They investigated the effect of liquid viscosities, up to 804 cP, and of pipe inclination between 0° and 5° on the drift velocities of large bubbles in stagnant liquid in a 0.022 m internal diameter pipe using capacitance measurements and image analysis techniques. Apart from the well-established general findings from previous researchers, i.e., the drift velocity increases with a decrease in oil viscosity, an increase in pipe diameter, and an increase in pipe inclination, the authors also observed the bubble velocity to be decreasing along the pipe for horizontal flow which agrees with the simulation results presented by Andreussi et al. [32] and Ramdin and Henkes [33]. Also, they observed the reduction of bubble velocity to gradually disappear as the pipe inclination is increased. However, the observed trends of the bubble velocities along the pipe were not regular. So, they mentioned the effects of pipe misalignments might have on the bubble velocity measurements (low value data) along the pipe.

This work presents the results of experimental investigations carried out, using light diode detectors and visualization techniques with high speed camera, targeting the behaviour of a single elongated bubble in oil viscosity with nominal values of 160 cP and 1140 cP in 0.099 m and 0.057 m internal diameter pipes inclined at angles between 1° and 7.5°. The new collected data of drift velocity can contribute to improve the general knowledge of pipe inclination and viscosity dependency in drift velocity correlations. Some of the outcomes have been reported in Livinus et al. [23], but with little details. In addition, obtaining data on the bubble characteristics - shape, length, void fraction and drift velocity, may help for the development and validation of numerical models, including Computational Fluid Dynamics (CFD) based models.

2.2 Experimental rig set-up and methodology

Experimental fluid characterisation was first carried out on the oils used as liquid phases as presented in Appendix B. Table B-1 summarises the experimental conditions under which the large bubble tests were performed, mostly under stagnant conditions. Figure 1 shows a plot of viscosity ratio against pipe length to pipe diameter ratio for this work and previous studies for slightly upwardly inclined pipes. The viscosity ratio, as defined in this work, is the ratio of the dynamic viscosity of a liquid to the dynamic viscosity of water, as a reference.

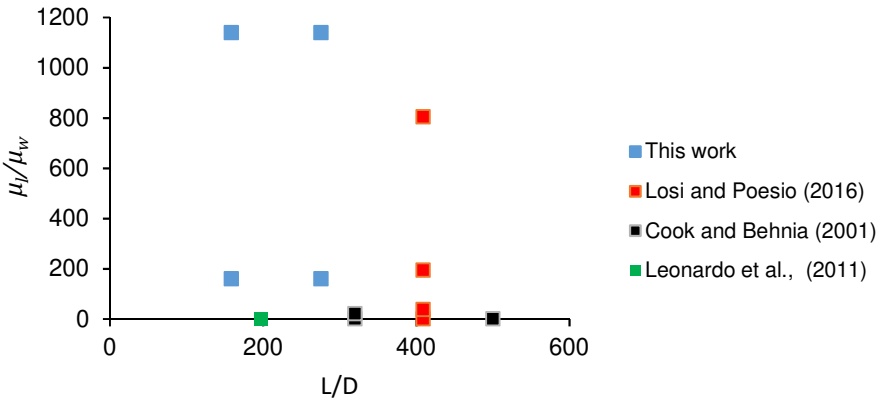

Figure 1: Plot of liquid viscosity ratio against ratio of pipe length to pipe diameter.

The low-pressure flow loop located at Institutt for Energiteknikk (IFE), as described by Bendiksen et al. [34] but with modifications, was used for the experiments, see the schematic presented in Figure 2, including dimensions. The loop consists of test pipe sections, a combined separator and storage tank, a low shear liquid pump, a gas supply and injector system, instrumentation and data acquisition systems. The test pipe sections have 0.099 m and 0.057 m internal diameter pipes, both of which being about 15.73m long transparent PVC/Perspex pipes mounted on a +/- 10° inclinable beam to the horizontal. The ratios of the test section length to pipe diameter (L/D) are about 159 and 276, respectively. Due to safety reasons, the maximum inclination angle, which was measured with a digital inclinometer, was 7.5°.

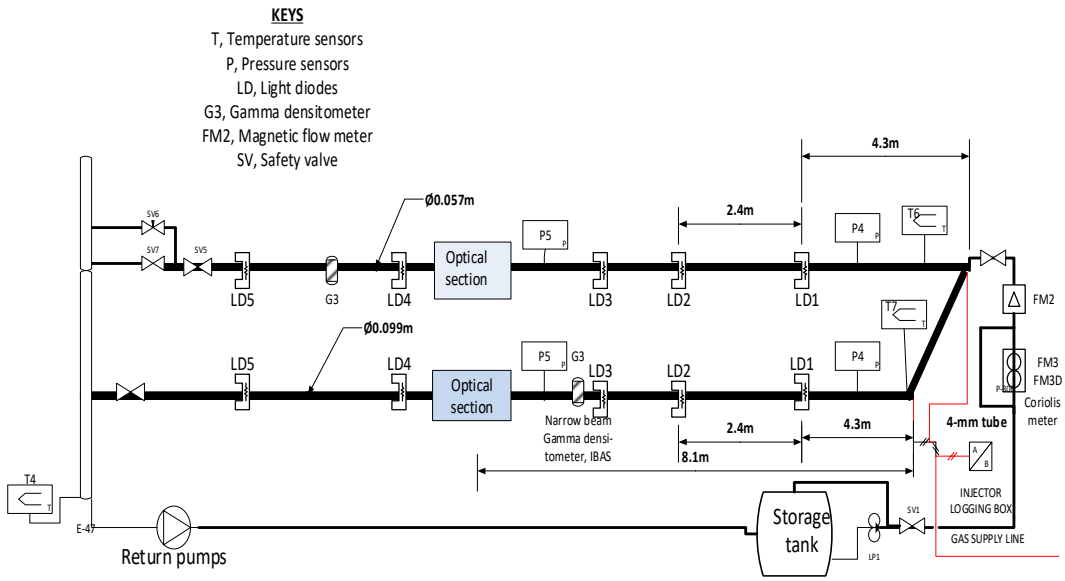

Figure 2: Schematic diagram of the test sections of the low-pressure loop

Figure 3 shows a sketch of the experimental set-up of the test pipe section with the oil filled beyond the position of the last diode detector but not to the end of the downstream of the pipe, as may be seen in the colour variations.

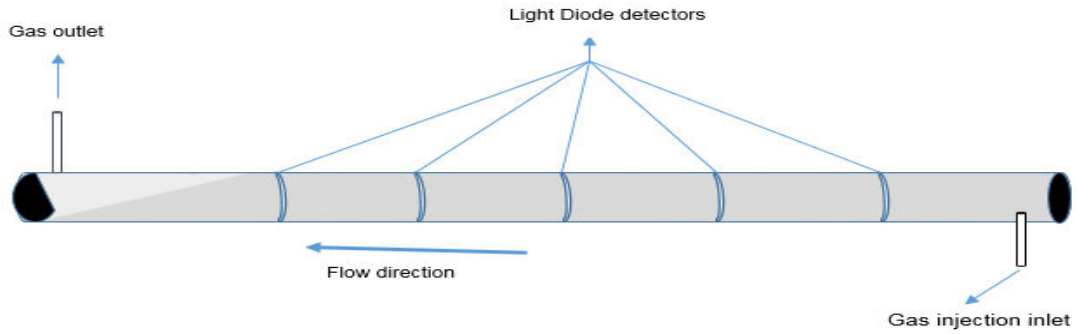

Figure 3: Sketch of the experimental set-up for the test pipe section, see Figure 2 for dimensions.

The gas injection system, operating at 10-bar maximum pressure, primarily consists of a pneumatic part turn actuator from Swagelok® Model MS-A15-4-DIN (manufactured by Air Torque S.p.A, Italy) and an actuator controller from Siemens LOGO! X50 logical unit (put into a case with 'Valve selection' and 'Start' button made by Ing. Pettersen, Drammen, Norway). A 4-mm internal diameter tube through the actuator forms the injection point - one connected to the nitrogen supply line and another connected slightly at the bottom of the test section through the actuator. For all experiments conducted, a single valve selection was made. By first programming the time required for the ball valve to remain open and setting the pressure of the nitrogen gas supply line at a fixed value (sometimes at 3.8-bar or 4-bar), a volume of gas is injected into the test section to ensure that a single bubble formation is achieved.

As there was no enough information about the downstream pressure of the injected gas in the test pipe, an estimation of the amount of gas injected for each test run has been performed. The equations for small bore orifice for gas flow as described by the American Society of Mechanical Engineers (ASME) [35] have been used to roughly estimate the flow rate of the injected gas at the point of injection. To minimize error, the ratio of differential pressure (Δp) divided by upstream pressure (P) is assumed not to exceed 0.25 (measured in the same engineering units). Based on this rule, a common factor, m of 0.11 has been used to determine the downstream pressure (or the differential pressure). Finally, the assumed discharge coefficient, C is gotten by subtracting the factor, m from unity. Details are provided in appendix E. The accuracy of this method is thus expected to be greater or equal to 89%. The estimated rate is then multiplied by the valve opening time of the injector to determine the volume of gas injected into the test section of the pipe.

Detector diodes measurements, Five detector diodes, all connected to an electric circuit almost similar to that of Bendiksen [2], were positioned exactly diametrically on the outer pipe surface over five preselected distances of the pipe length to measure the bubble propagation rates of its front and tail,

and its length. The major components of the detector diode-system are the receiver, Honeywell® SD5443 silicon phototransistor; and the emitter, Honeywell® SE5470 AlGaAs infrared emitting diode. The voltage reading is about 4.5 Volts without the presence of gas bubble in the pure stagnant or flowing liquid. When gas bubble is present, the detector voltage drops to about 0.0 Volt. The distance between two adjacent diodes was mostly 2.4 m. Figure 4 depicts typical graphical results of the transit time of a large bubble measured by the five detector diodes, respectively.

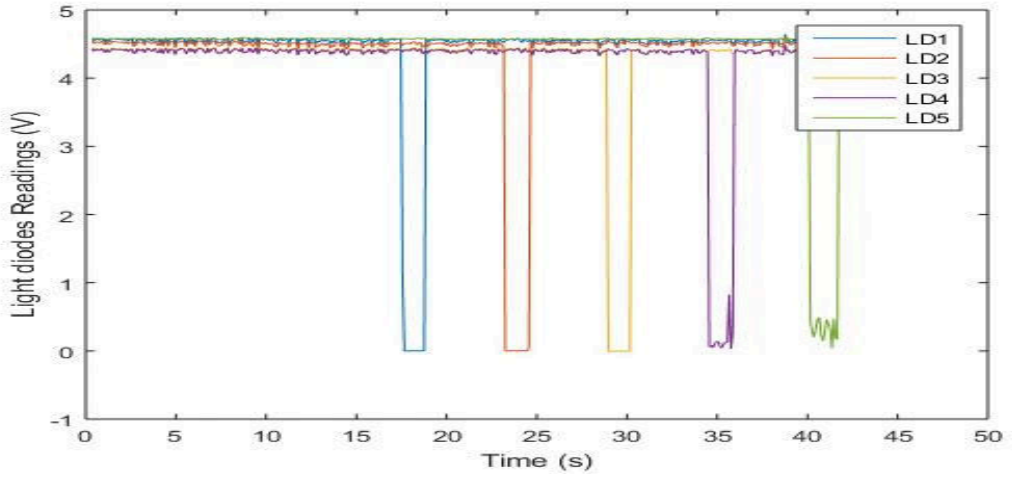

Figure 4: Typical graphical representation of the diode voltage readings for the five diodes

Prior to the start of the experiments, the test section was properly aligned and adjusted to be in the horizontal position. The positions of the light diode detectors on the surface of the test pipe were measured with a tape rule and recorded; it offered an uncertainty of 0.01 m. The high-speed camera, mounted opposite the observation box of the test pipe – about 8.1 m from the inlet of the gas injection, was turned on, its zoom lens adjusted for video recordings. For each inclination angle investigated, the test section was inclined to the angle of interest and its value measured with a smart inclinometer and recorded. The smart inclinometer has an uncertainty of 0.01°.

For the stagnant cases, the test section was filled with oil beyond the point of the last diode position, and the valves at the inlet and outlet were closed to trap the oil. A 4-mm tube was connected close to the outlet to remove the injected gas from the test section. With the help of the inclination beam, the test section was inclined to the angle of interest. In this study, 1°, 2.5°, 5° and 7.5° were investigated. The gas supply valve was opened first and adjusted to 3 – 4 bars before the valve opening time of the injector was set to achieve a particular volume of injected gas. A minimum of three injected gas volumes were successfully performed for each pipe inclination investigated, combined with the back pressure and different valve opening times. For each test, the flow was recorded with a high-speed camera. After the bubble had passed the last diode position, the time series logger was stopped. There was a waiting time of over one hour before the next test was conducted.

This approach was repeated for the entire planned test matrix. However, for the flowing cases, after performing the pre-experimental procedures similarly to the stagnant cases, the liquid pump was turned on and the bypass valve adjusted to achieve the desired liquid superficial velocity prior to the injection

of the nitrogen gas. When the work was completed, the liquid pump was turned off and all valves on the liquid feed line were closed.

To check the repeatability of the experiments, several experimental runs were conducted three times, and others were repeated twice. The percentage average standard deviation of the bubble velocity measurements was about 0.34%. The results therefore showed that a reasonable repeatability of the measurement parameters was achieved.

2.3 Bubble velocity and its length determination

The bubble velocity was estimated by smoothening the time series of the diodes' voltage readings obtained in a 100-Hertz operating logger into a 10-Hertz data. Comparative plots of the time series of the voltage readings from two diodes of interest, were created with MATLAB®, see Figure 5. The times taken for the diodes to detect the falling edge of the bubble nose and the edge of the bubble tail were then extracted.

The velocity of the bubble front, V_N, and bubble tail, V_T, were then obtained by the following simple equations:

$$V_N = \frac{\Delta x_i}{\Delta t_N}, V_T = \frac{\Delta x_i}{\Delta t_T} \tag{7}$$

where Δx_i is the distance between the two diodes of interest, and Δt_N is the time difference between the moment when the same edge of the bubble nose was detected by the diodes. Figure 5 depicts the marked interface corresponding to times (diode $i+1$) and (diode i).

Δt_T in Equation 7, is the time interval between the moments when the same edge of the bubble tail was detected by the diodes. The bubble velocity,V_B, was calculated by the average of the bubble nose velocity and the bubble tail velocity.

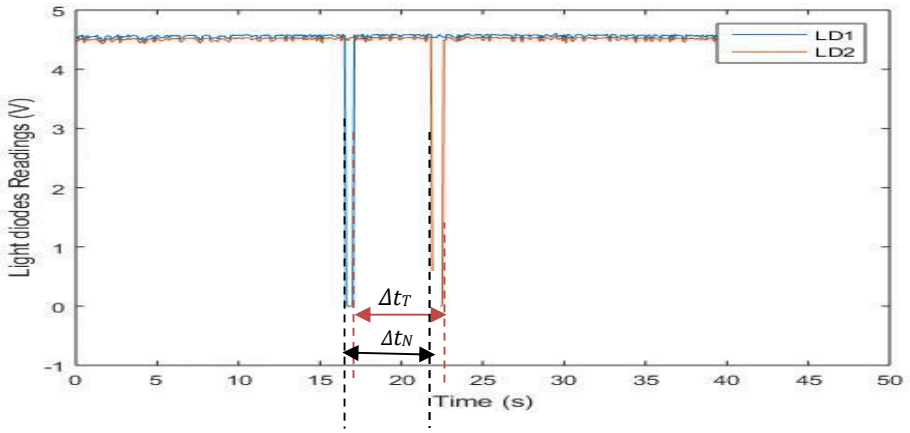

Figure 5: Marked transit time of the bubble movement

The change in the bubble velocity due to expansion effects as a result of gravity or frictional pressure drop was negligible when comparison was made for the number of diode pair considered. This therefore enables a definition of the overall average drift velocity as:

$$v_d = \frac{1}{N}\left[\sum_i^N V_B^i\right] \tag{8}$$

where, N is the number of diode pair considered, and the standard deviation is calculated as:

$$\Delta v_d = \sqrt{\frac{\sum_i^N \left(V_B^i - v_d\right)^2}{N-1}} \tag{9}$$

It is worth noting that the comparison of some of the first few measured bubble front velocities using the light diodes were compared with measurements obtained from a Photron Fastcam Analysis/ Photron Fastcam Viewer (PFA/PFV) technique. The outcome percentage discrepancy was insignificant, less than 4%, showing that the measurements were accurate. The readings from the detector diodes used in the determination of the bubble velocity were compared with the performance of the Photron Fastcam Analysis (PFA), an optional motion analysis tool, of the high-speed camera. The PFA of the Photron FASTCAM Viewer (PFV), version 1.2.0.0, was used to analyse the velocity of a few images taken with the high-speed camera by simply importing the image sequences directly from the PFV. Figure 6 shows the results comparison for experimental cases of 0.099 m internal diameter pipe with a 5° inclination from the horizontal. As can be seen, there is an excellent match of the results with an average discrepancy of 3%.

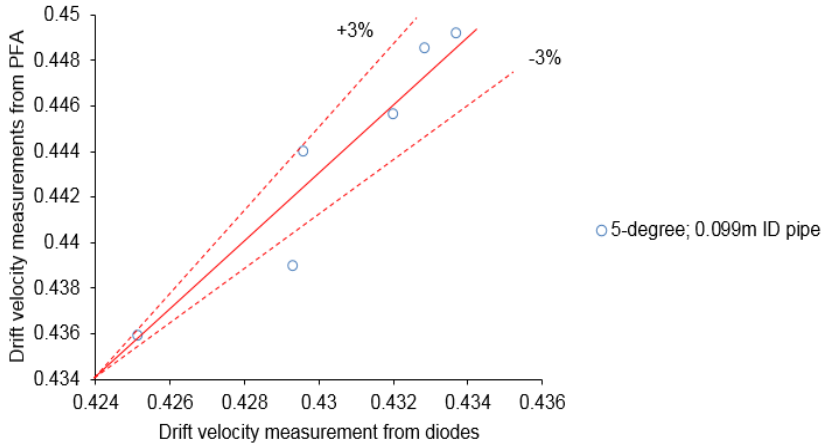

Figure 6: Drift velocity measurements comparison between diodes and PFA

The bubble length (Lb) was simply calculated by taking the average of the sum of the multiplication of the bubble velocity (V_B) and the average time interval (i.e for both Δt_N and Δt_T) for the number of diode pairs of interest.

There were uncertainties in the bubble velocity measurement from a pair of the diode detector system. These were mainly due to the uncertainties in the readings of the bubble nose positions at the two diodes of interest, and the averaging of the frequency of the time series of the diodes' signals. Such uncertainties were also present in the bubble length calculations. The uncertainty in the bubble velocity measurement is about ±3 %, and for the bubble length calculation, the average uncertainty is about 4%, but can be far greater than this value for the 1-degree pipe experiments because of the nature of the shape of the bubble

Video recordings and image processing. The high-speed videos recorded in this study were primarily for the bubble shape visualization; there were taken at a speed of 4000 frames per second with a 50mm zoom lens mounted opposite the observation box, which enclosed the viewing section of the test pipe into a transparent glass box. The glass box was filled with water to eliminate optical distortion due to the cylindrical shape of the pipe. The liquid height parameter, which is the ratio of the liquid depth (or height) and the pipe internal diameter, or the void fraction was obtained from the photographs with the aid of the image processing tool in MATLAB®, assuming a horizontally positioned pipe. Still images were extracted from the recorded video of an experimental run, cropped and uploaded into MATLAB® for post-processing. Three measurements or more were performed around the body of the bubble, and the average value presented. The uncertainty associated with the liquid height determination is about ±7%.

3.0 Experimental results presentation

The experimental data collected were processed to obtain the bubble drift velocity, the bubble shape and other parameters such as the Froude number and the liquid height parameter. Oil viscosities with nominal values of 160 cP and 1140 cP were used in the analyses, considering that the actual test viscosity range could be ±25 cP for the 160 cP oil viscosity and ±80 cP for the 1140 cP oil viscosity.

3.1 Bubble Shape and its length

A typical Taylor bubble possesses a nose, a body, a hydraulic jump and sometimes a tail. The shape of a bubble is greatly influenced by multiple parameters: the pipe diameter, viscosity, pipe inclination, liquid velocity, bubble length, etc. Figures C-1 and C-2 show some of the bubble shapes at different experimental conditions in stagnant and flowing liquid, respectively. In the stagnant liquid, the observed large bubble's nose always seemed to be prolate spheroid (or bell-shaped), with the tip of its nose close to the top of the pipe (as shown in Figure C-1(a-e)). Similarly, the tip of the bubble nose is also seen to be close to the top of the pipe at low mixture Froude number ($Fr_M < Fr_d = v_d/[(gD)(1-{}^{\rho_g}/_{\rho_l})]^{1/2}$) for the flowing cases (see Figure C-2a). However, at high mixture Froude number ($Fr_M = U_B/[(gD)(1-{}^{\rho_g}/_{\rho_l})]^{1/2}$), when the liquid velocity increased, the nose tended to move towards the centre of the pipe and its shape became quite flat (as shown in Figure C-2(b-d)). These observations

have been reported by previous researchers, Bendiksen [2], Fagundes et al. [3], Woods and Hanratty [13], Grenier et al. [14].

Depending on the pipe inclination, oil viscosities and volume of injected gas, or size of the bubble, the bubble's tail was observed to be either 'short-tapered with/without detached tiny bubbles' (STT and STwtB), or 'long-tapered' (LTT), while its body (i.e. at the interface between gas and liquid) was seen to be either 'curvy' or 'wavy' or flat. When the bubble was short, less than 3D, the bubble body seemed to exhibit a curvy pattern and its tail was short tapered without any detached tiny bubbles. For a pipe inclination below 2.5° and when the bubble length increased, the body was seen to exhibit a wavy pattern with a decreasing amplitude, and its tail tended to be long tapered. Above 2.5°, the bubble's body was flat, and its tail was short tapered, without any detached tiny bubbles for oil viscosity of 1140 cP, but with detached tiny bubbles for oil viscosity of 160 cP.

Bubble lengths greater than 20D and up to about 60D were observed in the 0.057 m internal diameter pipe. Under the same operating conditions, the maximum bubble length obtained for the 0.099 m internal diameter pipe was less than 15D.

3.2 Bubble drift velocity

The effect of viscosity, pipe diameter and pipe inclination on the drift velocity of elongated bubble in stagnant liquid in pipes has been summarised in Figure 7, using the dimensionless drift velocity; the Froude number. The results obtained show that the drift velocity increases with the increase of pipe inclination and pipe diameter but decreases with the increase of oil viscosity. These observations are in agreement with the findings of previous researchers, e.g. Jeyachandra et al. [4], Losi and Poesio [5], Gokcal et al. [10], and Moreiras et al. [28]. For the 0.057 m internal diameter pipe, the drift velocity slightly increases with the increase of the pipe inclination for both the oil viscosity of 160 cP. There is a significant drift velocity increase with the increase of the pipe inclination, especially between 1° and 5°, for the oil viscosity of 1140 cP. Similar trends, as observed in the 0.057 m internal diameter pipe, are also seen for the relationships of the drift velocity against the pipe inclination for the 0.099 m internal diameter pipe and the oil viscosities of 160 cP and 1140 cP. Error bars included in the plot, representing the upper and lower limits of the reported measured data for the varying bubble volume injected for a particular pipe inclination and pipe diameter, show a large variation in the measured drift velocity data for a pipe inclination of 1° for both oil viscosities. The discrepancy is however higher for the oil viscosity of 160 cP in the 0.099 m internal diameter pipe. A high discrepancy can also be seen for the data associated with the oil viscosity of 1140 cP in the 0.099 m for pipe inclinations between 1° and 2.5°. These variations could be the result of the deceleration of the bubble as it moves and expands along the pipe. Numerical simulation studies by Andreussi et al. [32], Ramdin and Henkes [33] and Kroes and Henkes [36], have shown that, for large liquid viscosity, the drift velocity of a bubble penetrating in a horizontal draining pipe decreases along the pipe. Losi and Poesio [5] pointed out that the reduction of the velocity can be attributed to the effect of growth in wall shear stresses in the liquid phase, which

drain an increasingly amount of the gravitational potential energy available in the difference of level in the nose of the bubble, needed for motion.

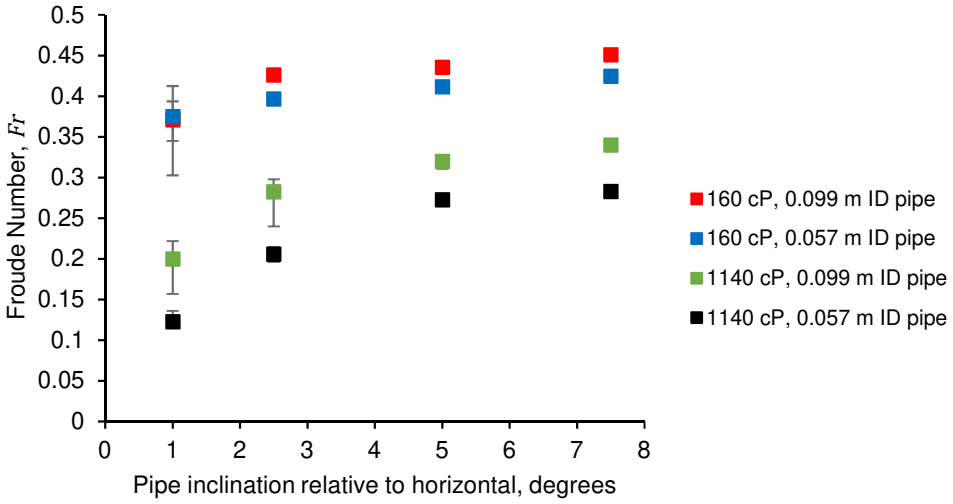

Figure 7: Effect of viscosity, pipe inclination and pipe ID on drift velocity expressed in Froude Number

The behaviour of the determined drift velocities of the elongated bubble along the pipe are shown from Figures 8 to 11 (plots of dimensionless drift velocity against dimensionless pipe length at diode detectors- 2, 3, 4, 5 positions from gas inlet injection point). As can be seen there are reductions of the values of drift velocity along the pipes for inclinations below 2.5° and particularly for the internal diameter pipe of 0.057 m. However, this observed trend is not consistent, especially approaching the downstream end of the pipe. This may generally due to the effects of the disturbances from pipe misalignment that might have occurred due to the reaction of the test pipe during the gas injection.

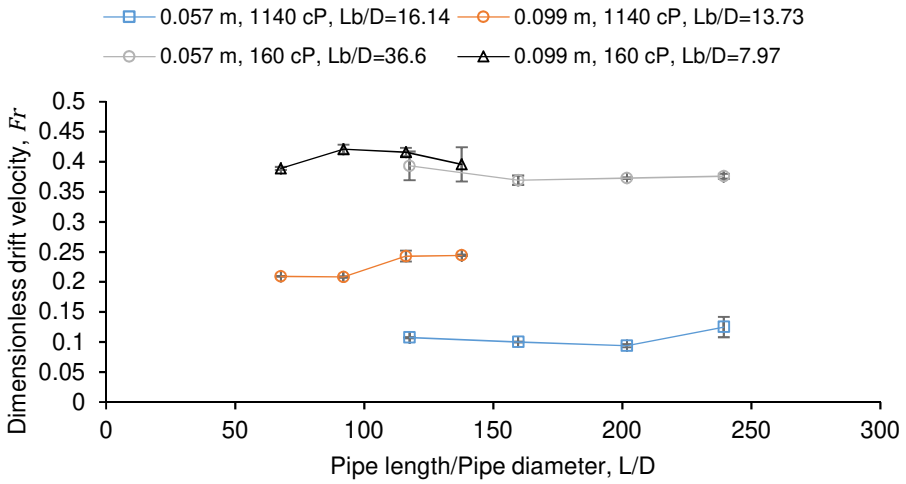

Figure 8: Drift velocities along the pipe of 1° inclination

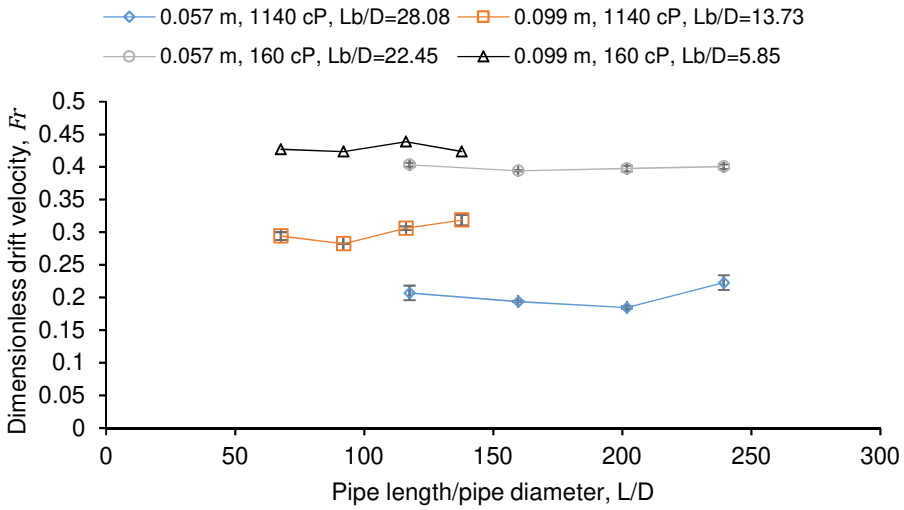

Figure 9: Drift velocities along the pipe of 2.5° inclination

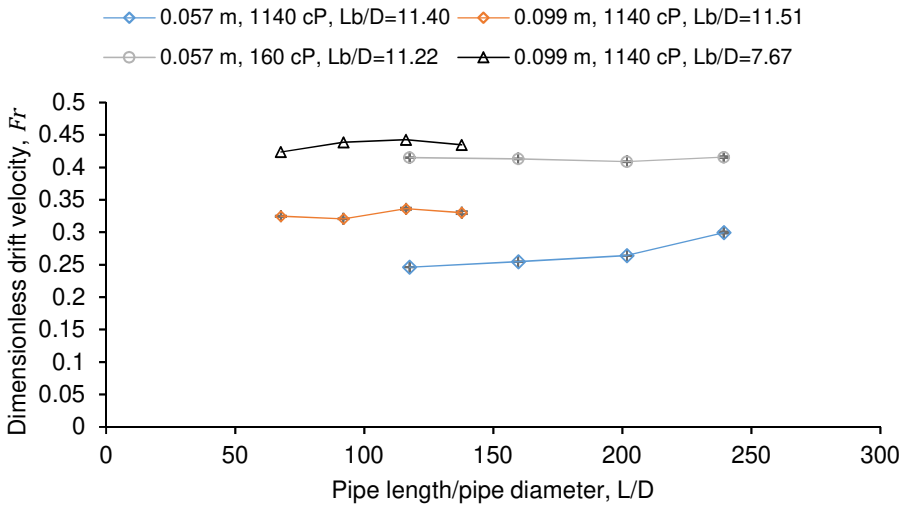

Figure 10: Drift velocities along the pipe of 5° inclination

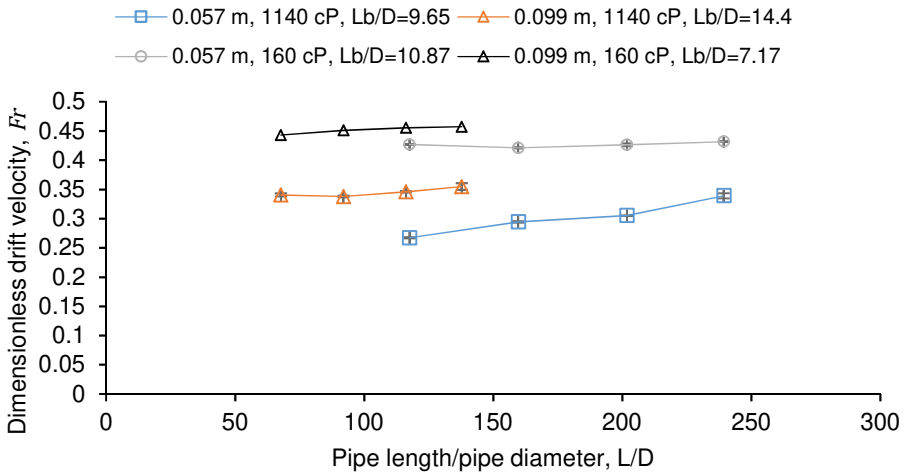

Figure 11: Drift velocities along the pipe of 7.5° inclination

The behaviour of the long gas bubble drift velocity for different injected gas volumes at each inclination are presented from Figures 12 to 15. The Figures also show plots of the drift velocity against the bubble size in dimensionless form (Lb/D). Looking at those figures, it seems that there is a slight influence of gas volume on the drift velocity. Examining the effect of the size of the injected gas volume for both oils in the 0.099 m diameter pipe, and for the 160 cP oil in the 0.057 m diameter pipe, when the pipe is inclined at 1° and 2.5° relative to horizontal, there is a slight influence (increasing trend) until the bubble size becomes greater than about five times the size of the pipe internal diameter. This could mean that the bubble requires a stronger drive to overcome the resistance offered by the high viscous fluid. This seems to be in line with the Zukoski's [11] hypothesis for vertical flow that the propagation velocity is independent of the length as long as the volume of the bubble corresponds to a cylinder with the tube radius and a length of 3 tube radii. This also seems to agree with the findings of Spedding and Nguyen [12]. However, the observation of the effect of bubble volume (or size) on the drift velocity for a higher viscous oil -1140 cP in the 0.057 m diameter pipe, seems to indicate a decreasing trend, as the bubble volume (or size) increases. This may be due to the high resistance offered by the viscous oil against the buoyancy force of the bubble dynamics.

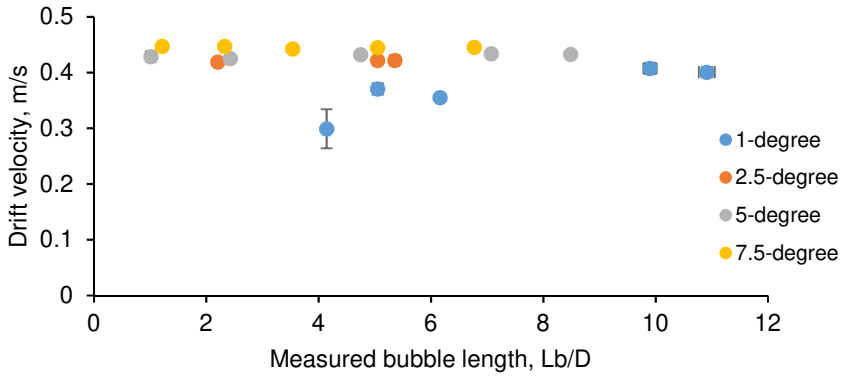

Figure 12: Effect of size of gas bubble on drift velocity for 160 cP Oil in 0.099 m ID pipe

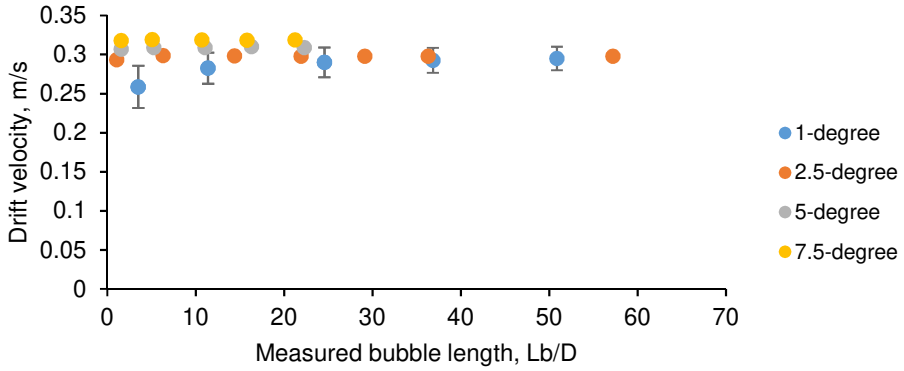

Figure 13: Effect of size of gas bubble on drift velocity for 160 cP oil in 0.057 m ID pipe

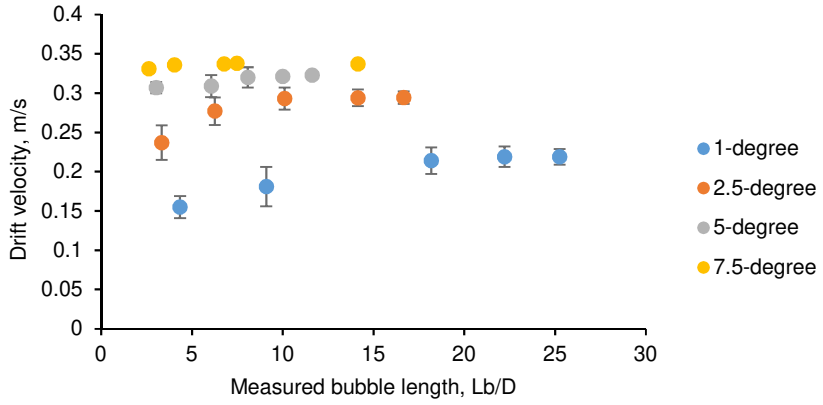

Figure 14: Effect of injected gas bubble size on drift velocity for 1140 cP oil in 0.099 m ID pipe

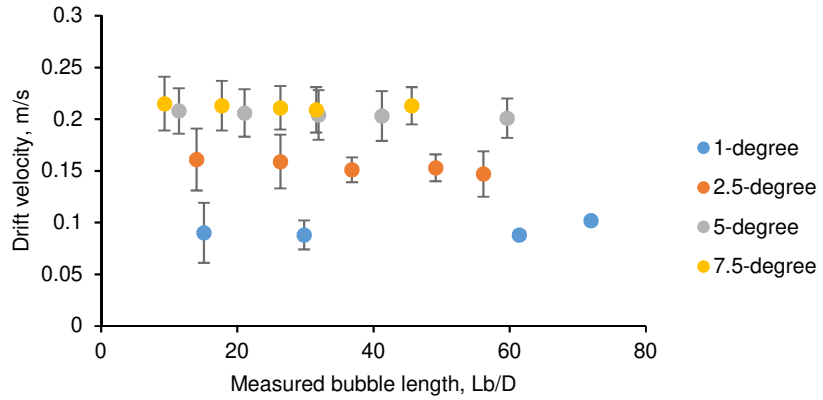

Figure 15: Effect of injected gas bubble size on drift velocity for 1140 cP oil in 0.057 m ID pipe

3.3 Liquid height parameter

The experimental liquid height parameters were determined from images taken with the high-speed camera at about 8.1 m from the inlet of the gas injection of the test pipes. The liquid height parameter is the ratio of the liquid depth (or height) and the pipe internal diameter. At high viscosity liquid, there is an increased resistance for the bubble to penetrate the oil, thereby reducing the bubble fraction, and increasing the liquid height. But with an increasing pipe inclination, the gravitational forces enable the bubble to penetrate deeper into the oil.

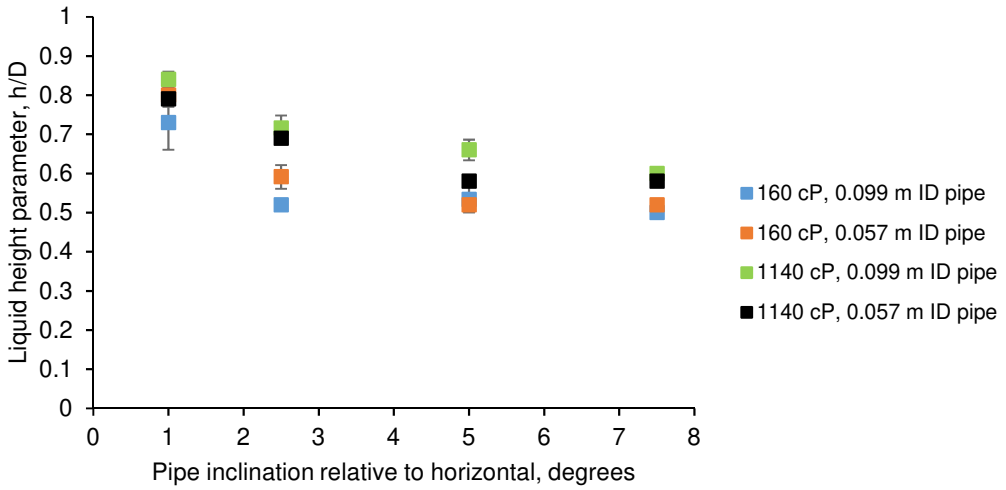

Figure 16: Liquid height parameter against pipe inclination

Figures 16 shows the relationships between the average liquid height parameter along with the standard deviation and pipe inclination for the two oil viscosities for the 0.057 m and 0.099 m internal pipe diameters. The liquid height parameter is seen to be decreasing for an increasing pipe inclination. It is higher for the oil viscosity of 1140 cP than for the 160 cP oil viscosity under the same pipe conditions.

3.4 Bubble velocity for the flowing cases

Very few experiments were conducted for the flowing case. These were performed in the 160 cP oil with superficial velocities varying from 0.1 to 0.32 m/s for the 0.099 m internal diameter pipe. A plot of the measured bubble velocity against the liquid velocity was made for each pipe inclination, and the drift velocity was obtained by extrapolating the bubble velocity to zero liquid velocity, see Figures 17. This approach is generally modelled based on the drift flux method of Nicklin et al. [16] presented earlier in Equation 1.

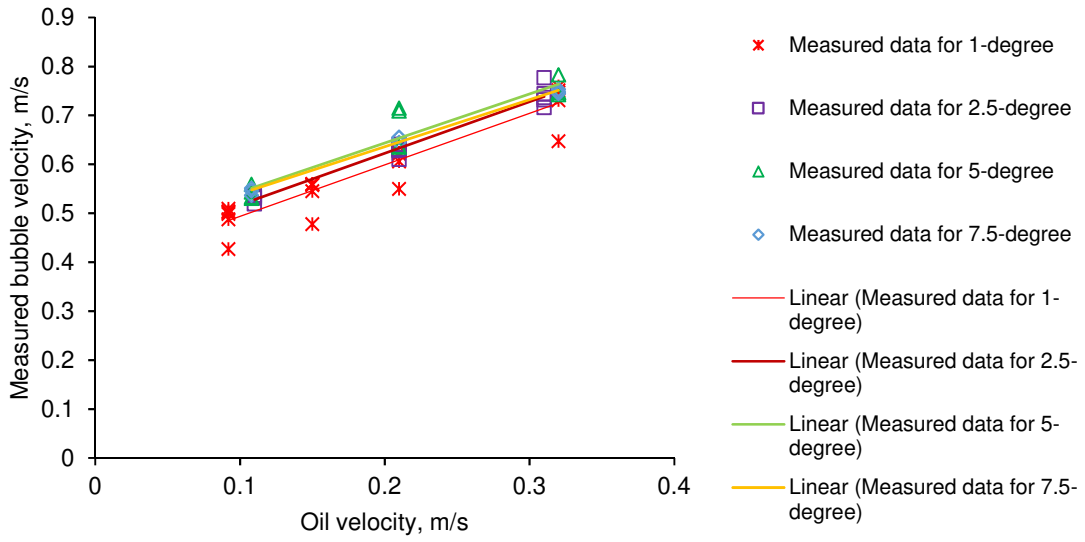

Figure 17: Bubble velocity vs liquid velocity for 160cP oil in 0.099m ID pipe

$$U_B = 1.0526v_m + 0.3884 \quad (10)$$

$$U_B = 1.051v_m + 0.4125 \quad (11)$$

$$U_B = 1.0024v_m + 0.4434 \quad (12)$$

$$U_B = 0.9613v_m + 0.4439 \quad (13)$$

The equations 10 through 13 represent the best fit equations for 1°, 2.5°, 5°, and 7.5°, respectively. The constants for these equations are the drift velocities of the long bubbles for the different pipe inclinations. As observed from all plots, the bubble velocity varies linearly with the liquid velocity with an average R^2-value of 0.93. The velocity distribution parameter, C_o is observed to slightly decrease as the pipe inclination increases. This parameter ranges from 0.9612 to 1.052. The velocity distribution parameter is plotted against the mixture Froude number for the individual test case. This is presented in Figure 18. The average value is seen to be 1.02, with a standard deviation of 0.15. About an average velocity distribution parameter of 1.05 has been reported in several studies, e.g. Jeyachandra et al. [4] and Diaz [37]. The four points with clear visible deviation from the straight lines in Figure 17, represent bubbles with size from the least gas injection volumes. Figure 19 shows a comparison plot of the drift velocity in terms of the Froude numbers against the pipe inclination for the 160 cP flowing oil and its stagnant case in 0.099 m internal diameter pipe. The results are similar for the various pipe inclination under study,

except for the 1-degree with noticeable discrepancy. However, the drift velocity for the flowing case of the 1-degree is still within the bandwidth of the results obtained for the stagnant case.

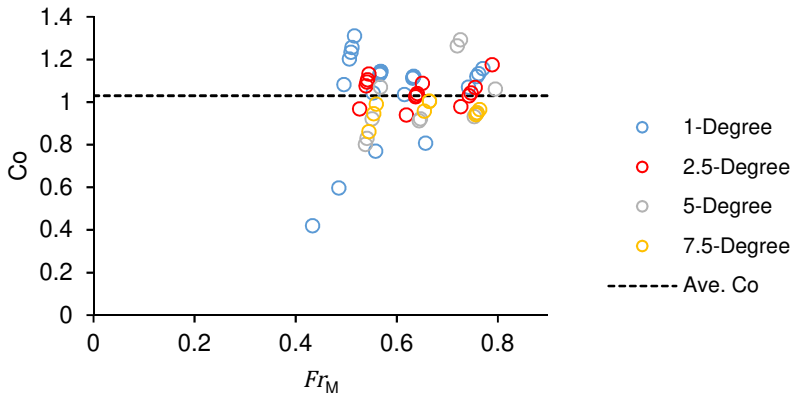

Figure 18: Velocity distribution parameters against Froude number for 160 cP flowing oil

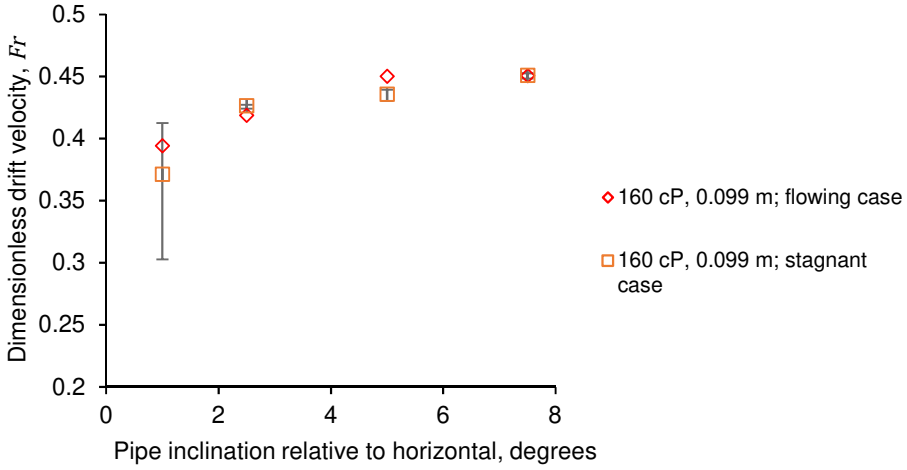

Figure 19: Effect of pipe inclination and pipe ID on drift velocity for both 160 cP flowing oil and stagnant oil

4.0 Experimental drift velocity results comparison with correlations predictions

The accurate prediction of drift velocity is essential in the modelling of multiphase flow in pipelines. In 1965, Zuber and Findlay confirmed the Drift flux relationship in Equation (1) for vertical flow in annular and slug flow. Franca and Lahey [38] using air–water experimental data verified the use of the Drift flux model for all flow patterns observed in horizontal gas–liquid flow. In 2009, Danielson and Fan [39] showed that this relationship is valid for stratified, annular, slug and dispersed bubble flows in a large diameter, horizontal and high pressure system. There are several drift velocity correlations proposed till date. However, there is need to improve on multiphase pipeline simulators in aiding the design and operations of both light and heavy oil production, processing and transportation facilities. Performance

evaluations of some of the bubble velocity correlations without the void fraction parameter may be found in different past works, see Jeyachandra et al. [4], Viana et al. [21], Livinus et al. [23] and Moreiras et al. [28]. Performance assessments of some drift velocity correlations with void fraction parameter may be found in Bhagwat and Ghajar [40].The documented experimental drift velocity results has been compared with the following bubble velocity correlations summarised in Table D-3: Jeyachandra et al. [4] model, Moreiras et al. [28] model and the revised Livinus et al. [23].

Jeyachandra et al. [4] model was formulated for any pipe inclination, similar to Bendiksen's [2] model, but in terms of Froude number, see Equation D-2a. The drift velocity for vertical flows was determined using the Joseph [41] model (Equation D-2c). For horizontal flow, the Froude number was expressed in exponential form in terms of viscosity number and Eötvös number, see Equation D-2b. In terms of Froude number, the predictions are quite in good agreement with the measured Froude numbers. Over 95% of the predictions are in the ±20% error range, see Figure 20(a). The predictions from Moreiras et al. [28] model summarised in Equations D-3(a-e) are not really encouraging, especially for the 1140 cP measured results. Measured results for the liquid viscosity of 160 cP are predicted within the ±40% error bandwidth while most of the measured results for the 1140 cP are above the ±40% error range, as may be seen in Figure 20(b). The model is valid for pipe internal diameter greater than or equal to 0.0373 m, and was developed using their own experimental data and limited data from the literature for pipe diameters between 0.0373 m and 0.178 m.

The modified model of Livinus et al. [23], see Equations D-4(a-f), was based on the fitting of a third-degree polynomial, considering the log-log relationship between the Froude number and a combination of the Eötvös number and the buoyancy Reynolds number, to a large gathered dataset. The curve fitting was considered for excellently matching the vertical flow and horizontal flow data and for having the least percentage error spread. The correlations predicted over 95% of the measured results in the ±20% error spread, as presented in Figure 20(c).

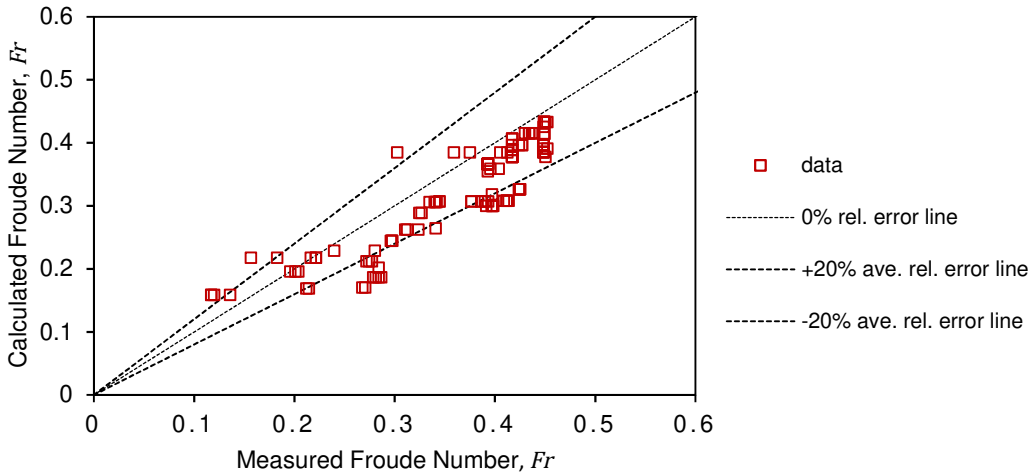

(a) Jeyachandra et al [4] model vs Measured results

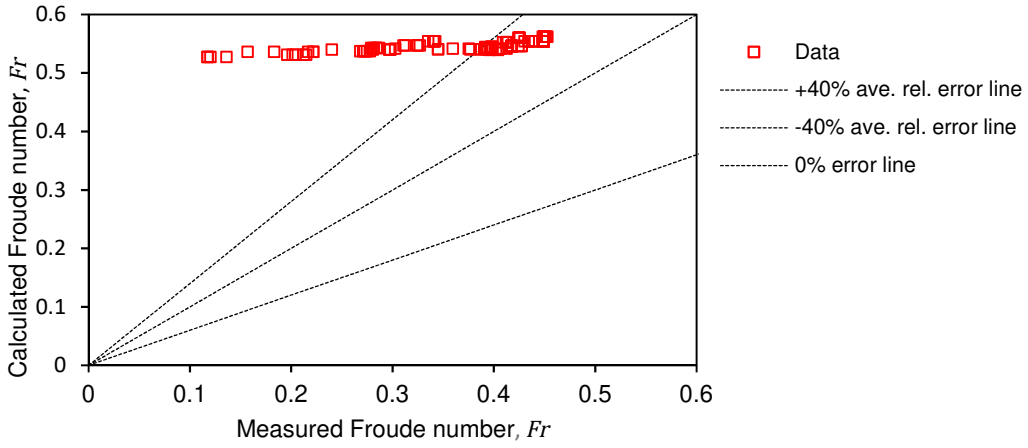

(b) Moreiras et al. [28] model vs Measured results

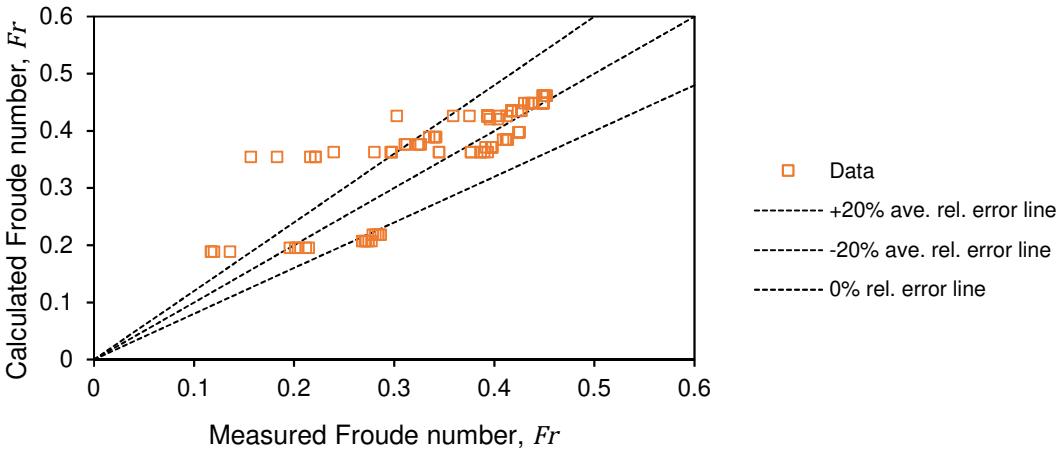

(c) Livinus et al. [23] modified model vs Measured results

Figure 20: Results comparisons with model predictions

Conclusion

Elongated bubble experiments in a low-pressure flow loop have been conducted with nominal oil viscosities of 160 cP and 1140 cP in 0.099 m and 0.057 m internal diameter pipes inclined at angles between 1 and 7.5 degrees to horizontal. In all cases, it was observed that the pipe diameter, pipe inclination, and oil viscosity affected the drift velocity of the elongated bubble. Also the bubble size, when it was less 5D, had effect on the drift velocity in the high viscous liquid. A large variation in the measured drift velocity data for pipe inclination of 1° for both oil viscosities was observed. The discrepancy was however higher for the oil viscosity of 160 cP in the 0.099 m internal diameter pipe. High discrepancy may also be seen for the data associated with the oil viscosity of 1140 cP in the 0.099 m for pipe inclination between 1° and 2.5°. The variations of the measured drift velocity might be due to the decelerations of the bubble as it moved and expanded along the pipe. The liquid height parameter was seen to be decreasing for increasing pipe inclination. The liquid height parameter was higher for

the oil viscosity of 1140 cP than for the 160 cP oil viscosity under the same pipe conditions. The shape of the bubble was greatly influenced by multiple parameters: the pipe diameter, viscosity, pipe inclination, liquid velocity, bubble length. For instance, depending on the pipe inclination, oil viscosities and volume of gas injected, or the size of the bubble, the bubble's tail was observed to be either 'short-tapered with/without detached tiny bubbles' (STT and STwtB), or 'long-tapered' (LTT).

Three recently developed drift velocity correlations are compared with the experimental drift velocity data. The Jeyachandra et al. [4] model and the revised Livinus et al. [23] model result in better predictions than the Moreiras et al. [28] model.

Recommendation. From the analyses of the experimental data, a relationship between the volume of gas injected and the length of the bubble was identified. Unfortunately, the injected gas was estimated. Installing a gas meter or having a known gas volume in a pressurized gas canister as a source connected to the injection system is thus recommended for future work to provide better means of quantifying the gas volume injected in the system.

Acknowledgements

The authors would like to thank the Consortium on Transient and Complex Multiphase Flows and Flow Assurance (TMF) for their in-kind support, and they acknowledge the support from ASCOMP; BP Exploration; Cameron Technology & Development; CD Adapco (now Siemens); Chevron; KBC (FEESA); FORSYS; INTECSEA; Institutt for Energiteknikk (IFE); Kongsberg Oil & Gas Technologies; Wood Group Kenny; Petrobras; Schlumberger Information Solutions; Shell; SINTEF; Statoil and TOTAL. The Authors wish to express their sincere gratitude to Morten Langsholt, Karin Hald, Jan Nossen, Karsten Opel, and Hans-Gunnar Sleipnæs for the support received from the Department of Process and Fluid Flow Technology, Institutt for Energiteknikk (IFE). The authors also acknowledge the support received from Prof. Hoi Yeung and Dr. Liyun Lao at Cranfield University.

References

[1] J. Fabre, A. Liné, Modeling of two-phase slug flow, Annu. Rev. Fluid Mech. 24 (1992) 21–46.

[2] K.H. Bendiksen, An experimental investigation of the motion of long bubbles in inclined tubes, International Journal of Multiphase Flow 10 (4) (1984) 467–483.

[3] J.R.N. Fagundes, J. Fabre, and L. Peresson, Shape of long bubbles in horizontal slug flow, International Journal of Multiphase Flow 25 (6-7) (1999) 1129–1160.

[4] B.C. Jeyachandra, B. Gokcal, A. Al-Sarkhi, C. Sarica, and A. Sharma, Drift-velocity closure relationships for slug two-phase high-viscosity oil flow in pipes, SPE Journal 17 (2) (2012) 593 - 601.

[5] G. Losi, and P. Poesio, An experimental investigation on the effect of viscosity on bubbles moving in horizontal and slightly inclined pipes, Experimental Thermal and Fluid Science 75 (2016) 77–88.

[6] M.E. Weber, A. Alarie, and M.E. Ryan, Velocities of extended bubbles in inclined tubes. Chemical Engineering Science 41 (9) (1986) 2235–2240.

[7] A. Hasan, and C. Kabir, Predicting multiphase flow behaviour in a deviated well, SPE Production Engineering 3 (4) (1988) 474 - 482.

[8] E.C. Shosho, and M.E. Ryan, An experimental study of the motion of long bubbles in inclined tubes, Chemical Engineering Science 56 (6) (2001) 2191–2204.

[9] R. Van Hout, D. Barnea, and L. Shemer, Translational velocities of elongated bubbles in continuous slug flow, International Journal of Multiphase Flow 28 (8) (2002) 1333–1350.

[10] B. Gokcal, A. S. Al-Sarkhi, and C. Sarica, Effects of high oil viscosity on drift velocity for upward inclined pipes, SPE Annual Technical Conference and Exhibition, ATCE, September 21-24 (2008), Denver, Colorado, USA.

[11] E.E. Zukoski, Influence of viscosity, surface tension, and inclination angle on motion of long bubbles in closed tubes, Journal of Fluid Mechanics 25 (4) (1996) 821.

[12] P.L. Spedding, and V.T. Nguyen, Bubble rise and liquid content in horizontal and inclined tubes, Chemical Engineering Science 33 (8) (1978) 987–994.

[13] B.D. Woods, T.J. Hanratty, Relation of slug stability to shedding rate, International Journal of Multiphase Flow 22 (5) (1996) 809-828.

[14] P. Grenier, J. Fabre, J.R. Fagundes Netto, Slug flow in pipelines: recent advances and future developments, In: Proc. Eighth Int. Conf. on Multiphase Production, June 18-20, (1997) Cannes, France, Cranfield BHRG.

[15] M.A. Woldesemayat, and A.J. Ghajar, Comparison of void fraction correlations for different flow patterns in horizontal and upward inclined pipes, International Journal of Multiphase Flow 33 (4) (2007) 347 – 370.

[16] D.J. Nicklin, Two-phase bubble flow, Chemical Engineering Science 17 (9) (1962) 693–702.

[17] K.H. Bendiksen, On the motion of long bubbles in vertical tubes, International Journal of Multiphase Flow, 11 (6) (1985) 797–812.

[18] Y. Taitel,D. Barnea, Two-phase slug flow, Advances in Heat Transfer 20 (1990) 83–132.

[19] K.H. Bendiksen, D. Malnes, O.J. Nydal, On the modelling of slug flow, Chemical Engineering Communications 141-142 (1) (1996) 71–102.

[20] E.T. White, and R.H. Beardmore, The velocity of rise of single cylindrical air bubbles through liquids contained in vertical tubes, Chemical Engineering Science 17 (5) (1962) 351–361.

[21] F. Viana, R. Pardo, R. Yanez, J.L. Trallero, D.D. Joseph, Universal correlation for the rise velocity of long gas bubbles in round pipes, Journal of Fluid Mechanics 494 (2003) 379–398. DOI: 10.1017/S0022112003006165.

[22] E. Lizarraga-Garcia, J. Buongiorno, E. Al-Safran, D. Lakehal, A broadly-applicable unified closure relation for Taylor bubble rise velocity in pipes with stagnant liquid, International Journal of Multiphase Flow 89 (2017) 345–358.

[23] A. Livinus, P. Verdin, L. Lao, J. Nossen, M. Langsholt, H. Sleipnæs, Simplified generalised drift velocity correlation for elongated bubbles in liquid in pipes, Journal of Petroleum Science and Engineering 160 (2018) 106–118.

[24] G.A. Gregory, D.S. Scott, Correlation of liquid slug velocity and frequency in horizontal cocurrent gas–liquid slug flow, AIChE Journal 15 (6) (1969) 933–935.

[25] A.E. Dukler, M.G. Hubbard, A model for gas–liquid slug flow in horizontal and near horizontal tubes, Ind. Eng. Chem. Fundam. 14 (1975) 337–347.

[26] T.B. Benjamin, Gravity currents and related phenomena, Journal of Fluid Mechanics 31 (02) (1968) 209–248.

[27] M.E. Weber, Drift in intermittent two-phase flow in horizontal pipes, The Canadian Journal of Chemical Engineering 59 (3) (1981) 398–399.

[28] J. Moreiras, E. Pereyra, C. Sarica, and C.F. Torres, Unified drift velocity closure relationship for large bubbles rising in stagnant viscous fluids in pipes, Journal of Petroleum Science and Engineering 124 (2014) 359–366.

[29] M. Cook, and M. Behnia, Bubble motion during inclined intermittent flow, International Journal of Heat and Fluid Flow 22 (5) (2001) 543–551.

[30] A. Perron, L.I. Kiss, and S., Poncsák, An experimental investigation of the motion of single bubbles under a slightly inclined surface, International Journal of Multiphase Flow 32 (5) (2006) 606–622.

[31] M. S. Leonardo, C.F. Jurandyr, L.H.F. Jose, and S. Jian, Measurement of drift velocity of elongated bubbles in slight inclined circular tubes using a filtered ultrasonic technique, International Nuclear Atlantic Conference – INAC, 24 – 28 (October) 2011, Belo Horizonte, Brazil.

[32] P. Andreussi, M. Bonizzi, and A. Vignali, Motion of elongated gas bubbles over a horizontal liquid layer, 14th Int. Conf. Multiph. Prod. Technol., 17 – 19 (June) 2009, Cannes, France.

[33] M. Ramdin, and R. Henkes, Computational Fluid Dynamics Modeling of Benjamin and Taylor Bubbles in Two-Phase Flow in Pipes, Journal of Fluids Engineering 134 (4): 041303 (2012).

[34] K.H. Bendiksen, M. Langsholt, and L. Liu, An experimental investigation of the motion of long bubbles in high viscosity slug flow in horizontal pipes, International Journal of Multiphase Flow, 104, (2018) 60 - 73, https://doi.org/10.1016/j.ijmultiphaseflow.2018.03.010.

[35] American Society of Mechanical Engineers (ASME), 2001. Measurement of fluid flow using small bore precision orifice meters. ASME MFC-14M-2001.

[36] R.F. Kroes, and R. A. W.M. Henkes, CFD for the motion of elongated gas bubbles in viscous liquid, BHR Group - 9th North American Conference on Multiphase Technology (1) (2014) 283–298.

[37] M.J.C. Diaz, Bubble Translational Velocity in Horizontal Slug Flow, 109 (2016) Ph.D. Thesis. NTNU, Trondheim, Norway.

[38] H. Franca, R.T. Lahey, The use of drift flux techniques for the analysis of horizontal two phase flows. International Journal of Multiphase Flow 18 (6) (1992) 787–801.

[39] T.J. Danielson, Y. Fan, Relationship between mixture and two-fluid models, In: Proceedings of the BHR Group International Conference on Multiphase Production Technology, June 17–19, (2009) Cannes, France.

[40] S.M. Bhagwat, and A.J. Ghajar, A Flow Pattern Independent Drift Flux Model Based Void Fraction Correlation for a Wide Range of Gas-Liquid Two Phase Flow, International Journal of Multiphase Flow, 59 (February): (2014) 186–205.

[41] D.D. Joseph, Rise velocity of a spherical cap bubbles, Journal of Fluid Mechanics 488 (2003) 213–223.

[42] I.N. Alves, O. Shoham, and Y. Taitel, Drift velocity of elongated bubbles in inclined pipes, Chemical Engineering Science 48 (17) (1993) 3063–3070.

[43] P.S. Carew, N.H. Thomas, and A.B. Johnson, A physically based correlation for the effects of power law rheology and inclination on slug bubble rise velocity, International Journal of Multiphase Flow 21 (6) (1995) 1091–1106.

[44] R. Van Hout, A. Gulitski, D. Barnea, and L. Shemer, Experimental investigation of the velocity field induced by a Taylor bubble rising in stagnant water, International Journal of Multiphase Flow 28 (4) (2002) 579–596.

[45] H. Shi, J. Holmes, L. Diaz, L. Durlofsky, and K. Aziz, Drift-Flux Parameters for Three-Phase Steady-State Flow in Wellbores, SPE Journal, 10(June), (2005) 1–11.

[46] C. Kora, C. Sarica, H.Q. Zhang, and K. Fahd, Effects of High Oil Viscosity on Slug Liquid Holdup in Horizontal Pipes, SPE; Canadian Unconventional Resources Conference, 15 - 17 November, (2011), Calgary, Alberta, Canada.

[47] W.R. Oliveira, I.B. de Paula, F.J.W. Martins, P.S.C. Farias, and L.H. Azevedo, Bubble characterization in horizontal air–water intermittent flow, International Journal of Multiphase Flow 69 (2015) 18–30.

[48] H. Gu, and L. Guo, Bubble shape in horizontal and near horizontal intermittent flow, Annals of Nuclear Energy 80 (2015) 312–321.

Appendix A – Literature reviews of experimental studies on large bubble related flow

Table A-1: Some experimental studies on the characteristics of Large bubble related flow

Author	Fluid Properties	Pipe Information	Comments
Zukoski [11]	ρ_l = 1000 kg/m^3, $\mu_l = 1$ cP, $\sigma = 0.072$ N/m	θ = 0 – 90°, ID = 0.055 m, 0.178 m	Studied influence of viscosity and surface tension on bubble velocities, suggested a correlation for bubble velocity
Bendiksen [2]	ρ_l = 1000 kg/m^3, $\mu_l = 1$ cP, $\sigma = 0.072$ N/m	θ = -30 – 90°, ID = 0.0242 m, 0.192 m, 0.05 m.	Used diode detector to measure drift velocity in liquid flowing case, developed a drift velocity model
Weber et al. [6]	ρ_l = 1280 - 1410 kg/m^3, $\mu_l = 51.1 - 6120$ cP, $\sigma = 0.078$ - 0.087 N/m	θ = 0 – 90°, ID = 0.006 m, 0.0373 m	Developed a drift velocity model
Ibere et al. [42]	ρ_l = 800 kg/m^3, $\mu_l = 1.6$ cP, $\sigma = 0.028$ N/m	θ = 0 – 90°, ID = 0.051 m	Applied capacitance sensors to measure instantaneous liquid hold-up, drift velocity and bubble length
Carew et al. [43]	ρ_l = 1000 kg/m^3, $\mu_l = 1$ cP, $\sigma = 0.075 - 0.077$ N/m	θ = 0 – 90° , ID = 0.025 m, 0.045 m, 0.07m	Measured drift velocity with two infrared beams.
Fagundes et al. [3]	ρ_l = 1000 kg/m^3, $\mu_l = 1$ cP, $\sigma = 0.072$ N/m, $V_L = 0.1 - 2$ m/s	θ = 0°, ID = 0.053 m	Used five wire capacitance sensors to determine drift velocity, length and shape
Cook and Behnia [29]	ρ_l = 1000 kg/m^3, $\mu_l = 1$ cP, $\sigma = 0.072$ N/m	θ = 0 – 10° , ID = 0.032 m, 0.050 m	Measured drift velocity in stagnant and flowing liquid with conductance electrodes.
Van Hout et al. [9]	ρ_l = 1000 kg/m^3, $\mu_l = 1$ cP, $\sigma = 0.072$ N/m	θ = 0°, ID = 0.024 m, 0.054 m	Used optical fibre probes and image processing technique

			to determine translational velocities, developed a simple model for translational velocities.
Van Hout et al. [44]	ρ_l = 1000 kg/m^3, $\mu_l = 1$ cP, $\sigma = 0.072$ N/m	θ = 0°, ID = 0.024 m, 0.054 m	Used PIV measurement technique to determine the velocity field induced by a Taylor bubble in stagnant liquid
Shi et al. [45]	ρ_l = 1000 kg/m^3, 810 kg/m3, $\mu_l = 1 - 1.5$ cP, $\sigma = 0.072$ N/m	θ = 0 - 92°, ID = 0.15 m	
Perron et al.[30]	ρ_l = 1000 kg/m^3, $\mu_l = 1$ cP, $\sigma = 0.072$ N/m	θ = 0 - 10°, Plexiglass surface	Studied the effects of surface inclination and bubble volume on the terminal Froude number.
Gockal et al. [10]	ρ_l = 889 kg/m^3, $\mu_l = 107 - 1237$ cP, $\sigma = 0.029$ N/m	θ = 0 – 90°, ID = 0.0508 m	Measured drift velocity with two laser beams and sensors, developed a drift velocity model
Kora et al. [46]	ρ_l = 889 kg/m^3, $\mu_l = 587, 378, 257$ cP, $\sigma = 0.029$ N/m, $V_L = 0.1 - 0.8$ m/s	θ = 0°, ID = 0.0508 m	Measured liquid hold-up and liquid film height with capacitance sensors.
Leonardo et al. [31]	ρ_l = 1000 kg/m^3, $\mu_l = 1$ cP, $\sigma = 0.072$ N/m	θ = 2.5°, 5°, 10°, ID = 0.0254 m	Measured drift velocity using high speed ultrasonic filtered pulse echo system
Jeyachandra et al. [4]	ρ_l = 889 kg/m^3, $\mu_l = 154 - 574$ cP, $\sigma = 0.029 - 0.030$ N/m	θ = 0 – 90°, ID = 0.0508 m, 0.0762 m, 0.1524 m.	Measured drift velocity in stagnant liquid by two sensors, developed a drift velocity model.

Moreiras et al. [28]	ρ_l = 870 kg/m^3, $\mu_l = 39 - 166$ cP, $\sigma = 0.0275$ N/m	θ = 0 – 90°, ID = 0.0508 m	Used high speed camera to determine drift velocity, developed unified closure relationship for drift velocity from their data and published data with pipe range of 0.0373 – 0.178 m.
Oliveira et al. [47]	ρ_l = 1000 kg/m^3, $\mu_l = 1$ cP, $\sigma = 0.072$ N/m	θ = 0°, ID = 0.0508 m	Applied high speed camera and infrared gate sensors to characterise elongated bubbles.
Gu and Guo [48]	ρ_l = 1000 kg/m^3, $\mu_l = 1$ cP, $\sigma = 0.072$ N/m	θ = 0°, ID = 0.05 m	Experimentally study the shapes of Taylor bubbles using video camera and conductive probes.
Losi and Poesio [5]	ρ_l = 998, 860, 875, 886 kg/m^3, $\mu_l = 1, 35.7, 195, 804$ cP, $\sigma = 0.0717, 0.0263, 0.0267, 0.0151$ N/m	θ = 0 – 5^o , ID = 0.022 m, L = 9 m	Applied video camera and capacitance probe to observe the shapes and measure the drift velocity of long bubbles, respectively. Performs comparatives analyses of various drift velocity correlations on the measured data

Appendix B - Experimental fluid characterisation

Nitrogen gas, with a density of 1.17 kg/m^3 at 20°C and 101.325 N/m^2, was used as the injected gas. The oils used as liquid phases were Primol 352 and Castor Oil Virgin. The measurements of the Rheological properties of the liquids, the viscosity, shear stress and shear rate, were carried out using the Anton Paar Physica MCR 301 Rheometer, while the surface tensions were measured with surface tension ring probes. The effect of the temperature on the viscosity of the oils was analysed from 15°C to 25°C. Figure B-1 shows the temperature influence on the oil viscosity for the Primol 352. As can be seen from the curve fitting equation, the viscosity change is about 10cP per degree temperature change. Virtually all the experiments were performed at a measured temperature of approximately 21°C; this implies that the nominal oil viscosity used was 160 cP. The density of the oil was about 870 kg/m^3. The refractive index of the Primol 352 is 1.479.

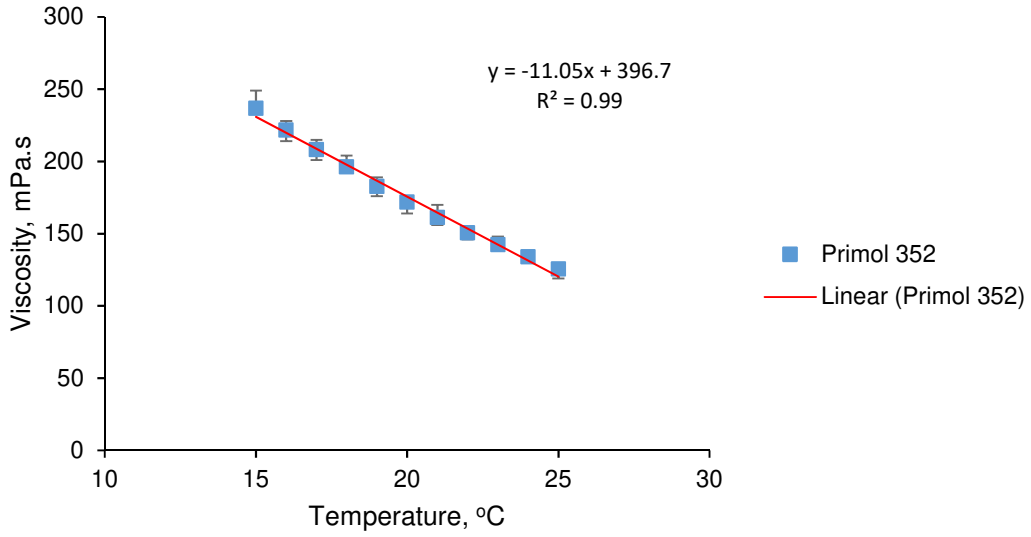

Figure B-1: Effect of temperature on the viscosity of Primol 352

The effect of temperature on the Castor Oil Virgin is highlighted in Figure B-2. As can be seen from the curve fitting equation, the viscosity change is about 86 cP per degree temperature change. All the experiments were performed at an average temperature of 19.2°C, implying a nominal oil viscosity of 1140 cP. The density of the oil considered was about 960 kg/m^3.

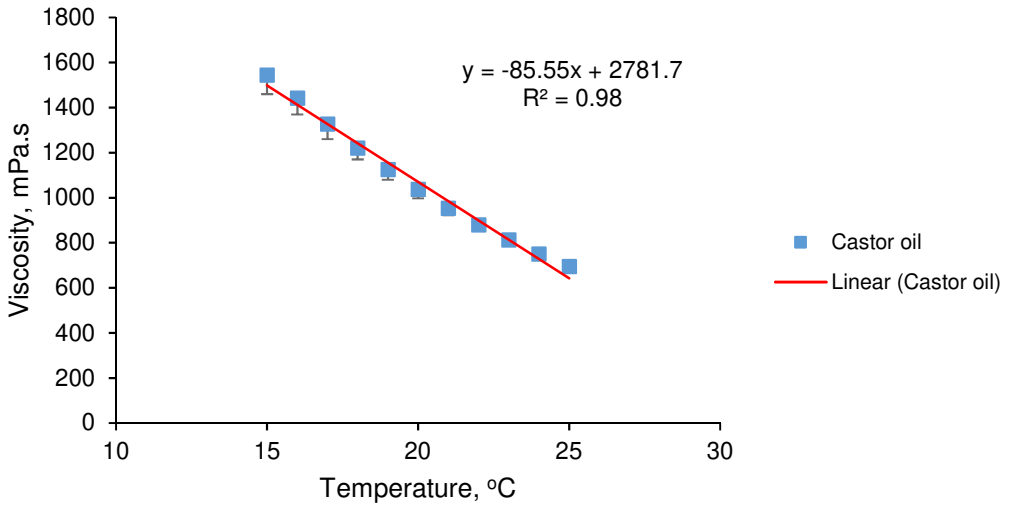

Figure B-2: Temperature effect on the viscosity of Castor Oil

The oils used in this study are Newtonian, based on the shear stress / shear rate analyses of the characterised fluids. The surface tensions at 20°C of the Primol 352 and Castor Oil Virgin are 0.027 N/m and 0.036 N/m, respectively, with an uncertainty of ± 0.001 N/m. Table B-2 summarises the experimental conditions under which the large bubble tests were performed, mostly under stagnant conditions. For the few flowing cases investigated, a temperature increase of 2-3 °C was noticed when performing a set of experiments using the viscosity oil with nominal value of 160 cP. However, for the stagnant cases, temperature variations were in the ±1 °C range.

Table B-2: Summary of experimental parameters

Parameters/Conditions	Values
Pipe length	15.73 m
Internal Pipe diameters	0.099 m, 0.057 m
Pipe inclinations relative to horizontal	1°, 2.5°, 5°, 7.5°
Oil density @ 20°C	870 kg/m^3, 960 kg/m^3
Oil viscosity @ 21°C, 19.2°C	160 cP, 1140 cP
Gas density	1.17 kg/m^3
Surface tension @ 20°C	0.027 N/m, 0.036 N/m

Appendix C – Bubble shape and its length

Some still images extracted, and cropped, from the recorded video of some experimental runs.

(a) 160 cP_0.099 m ID pipe_1degree, Lb/D = 10.90, Fr_d=0.4052, VOLgas = 0.004493 m^3, (LTT). Original image size: Height, 32.9 mm, and Width, 123.1 mm. Scaled dimension: Height, 84% and Width, 100%

(b) 160 cP_0.099 m ID pipe_2.5degree, Lb/D=5.05, Fr_d=0.4272, VOLgas = 0.002996 m^3, (STT). Original image size: Height, 67.9 mm, and Width, 223.4 mm. Scaled dimension: Height, 41% and Width, 53%

(c) 160 cP_0.099 m ID pipe_5degree, Lb/D=7.07, Fr_d=0.4394, VOLgas = 0.004493 m^3, (STwtB). Original image size: Height, 39 mm, and Width, 131.8 mm. Scaled dimension: Height, 80% and Width, 91%

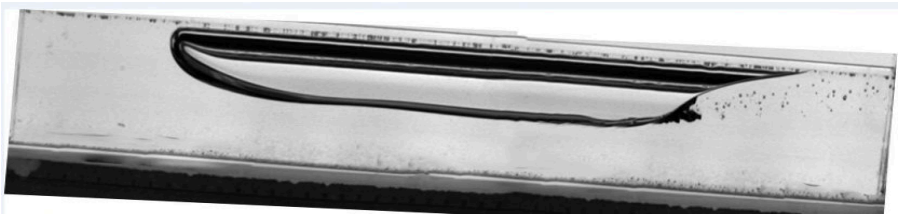

(d) 160 cP_0.057 m ID pipe_5degree, Lb/D=11.05, Fr_d=0.412, VOLgas = 0.001498 m^3, (STwtB). Original image size: Height, 71.5 mm, and Width, 219.8 mm. Scaled dimension: Height, 39% and Width, 54%

(e) 160 cP_0.099 m ID pipe_7.5degree, Lb/D=3.53, Fr_d=0.4483, VOLgas = 0.002995 m^3, (STwtB). Original image size: Height, 100.3 mm, and Width, 234.8 mm. Scaled dimension: Height, 27% and Width, 50%

Figure C-1: Some selected bubbles in stagnant liquid conditions.

(a) 2.5degree_Vso = 0.11 m/s, Lb/D=3.89, Fr_d=0.4176, VOLgas = 0.002246 m^3. Original image size: Height, 31 mm, and Width, 120.8 mm. Scaled dimension: Height, 93% and Width, 100%

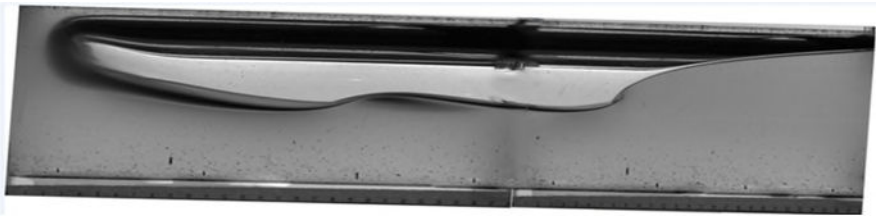

(b) 2.5degree_Vso = 0.21 m/s, Lb/D=3.324, Fr_d=0.4176, VOLgas = 0.002246 m^3. Original image size: Height, 31.2 mm, and Width, 115.7 mm. Scaled dimension: Height, 90% and Width, 100%

(c) 2.5degree_Vso = 0.31 m/s, Lb/D=5.824, Fr_d=0.4176, VOLgas = 0.004493 m^3. Original image size: Height, 32.9 mm, and Width, 122.46 mm. Scaled dimension: Height, 91% and Width, 100%

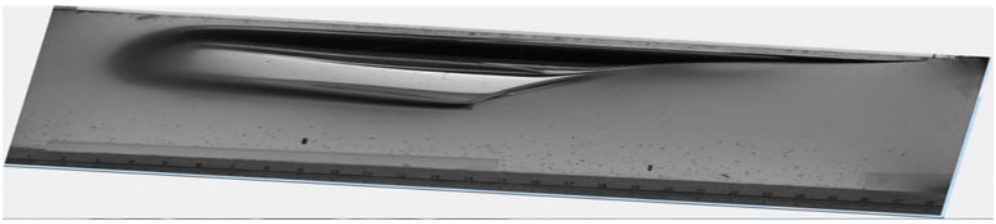

(d) 7.5deg_Vso = 0.32 m/s, Lb/D=1.02, Fr_d=0.4494, VOLgas = 0.0007488 m^3. Original image size: Height, 38.1 mm, and Width, 141.1 mm. Scaled dimension: Height, 74% and Width, 93%

Figure C-2: Some selected bubbles in flowing liquid conditions for 160 cP_0.099 m ID pipe

Appendix D – Drift velocity correlations evaluated under this work

The entire documented experimental drift velocity results has been compared with the following bubble velocity correlations summarised in Table D-3: Jeyachandra et al. [4] model, Moreiras et al. [28] model and the revised Livinus et al. [23].

Table D-3: Summary of bubble velocity correlations validated

Authors	Correlation/model	Range of validity	Equation No.
Jeyachandra et al. [4]	$Fr_\theta = Fr^h cos\theta + Fr^v sin\theta$	0^o – 90^o	D-2a
	$Fr^h = 0.53e^{-13.7N_{vis}^{0.46}Eo^{-0.1}}$		D-2b

	$$Fr^{v} = -\frac{8}{3}\mathrm{N}_{\mathrm{vis}} + \sqrt{\frac{2}{9}\frac{\rho_L}{\rho_L - \rho_G} + \frac{64}{9}\mathrm{N}_{\mathrm{vis}}^2}$$		D-2c
	$$\mathrm{N}_{\mathrm{vis}} = \mu\left(gD^3(\rho_l - \rho_g)\rho_l\right)^{-0.5}$$		D-2d
Moreiras et al. [28]	$$Fr_H = 0.54 - \frac{\mathrm{N}_{\mathrm{vis}}}{1.886 + 0.01443\mathrm{N}_{\mathrm{vis}}}$$	0° – 90°, D ≥ 0.0373 m	D-3a
	$$Fr_V = -\frac{8}{3}\mathrm{N}_{\mathrm{vis}} + \sqrt{\frac{2}{9}\frac{\rho_L}{\rho_L - \rho_G} + \frac{64}{9}\mathrm{N}_{\mathrm{vis}}^2} - \left(\frac{\sqrt{2}}{3} - 0.35\right)\sqrt{\frac{\rho_L}{\rho_L - \rho_G}}$$		D-3b
	$$Fr = Fr_H cos(\theta)^{1.2391} + Fr_V sin(\theta)^{1.2315} + Q$$		D-3c
	$$\mathrm{Q} = 0, \text{if } Fr_V - Fr_H < 0$$		D-3d
	Otherwise;		D-3e
	$$Q = 2.1589(Fr_V - Fr_H)^{0.70412} sin\theta(1 - sin\theta)$$		
Livinus et al. [23] modified	$$x = Log_{10}(REo)$$	0° – 90°	D-4a
	$$Fr^H = 10^{-m}$$		D-4b
	$$m = (-0.02861x^3) + (0.5987x^2) + (-4.139x) + 9.843$$		D-4c
	$$Fr^V = 10^{-n}$$		D-4d
	$$n = (-0.01386x^3) + (0.267x^2) + (-1.727x) + 4.167$$		D-4e
	$$Fr^{\theta} = Fr^H cos\theta + Fr^V sin\theta$$		D-4f

Appendix E – The equations for small bore orifice for gas flow calculations under this work

Equations used to estimate the flow rate of the injected gas at the point of injection for the experimental work are presented in this appendix.

The equations for small bore orifice for gas flow as described by ASME [35] have been used to estimate the flow rate of the injected gas at the point of injection. The estimated actual flow rate, Q_a is then multiply by the valve opening time, t of the injector to determine the volume of gas injected into the test section of the pipe.

Some assumptions were made in the use of the equations for small bore orifice for gas flow. A typical gas isentropic exponent, K is assumed to be 1.4. To minimize error, the ratio of differential pressure (Δp) divided by upstream pressure (P) is assumed not to exceed 0.25 (measured in the same engineering units). Based on this rule, a common factor, m of 0.11 has been used to determine the

downstream pressure (or the differential pressure). Finally, the assumed discharge coefficient, C is gotten by subtracting the factor, m from unity.

The equation below shows the formula used to obtain the factor, m. It is the volume of a single elongated bubble in the test pipe divided by the theoretical volume of the injected gas using ideal gas equation.

$$m = \frac{\alpha \pi r^2 L_B}{ZnR_c Tt/P} \quad \text{(E-1)}$$

where,

α, the fraction of a well-shaped single elongated bubble in the test pipe.

r, the radius of the test pipe, metres.

L_B, the length of a single elongated bubble in the test pipe, metres.

P, the gas supply line pressure, the upstream pressure, Pa.

T, the gas supply line temperature, Kelvin.

t, the time programmed for the actuator valve to remain open for a singular injection case, seconds.

n, the number of moles of gas = 1.

Z, the gas compressibility factor = 1.

R_c, the universal gas constant, = 8.3144621 m^3 Pa K^{-1} mol^{-1}.

The actual volumetric flow rate, Q_a of the injected gas is calculated by;

$$Q_a = \frac{Q_m}{\rho} \quad \text{(E-2)}$$

where,

Q_m, the mass flow rate of the injected gas. kg/s.

ρ, density of the injected gas at operating conditions, kg/m^3.

The mass flow rate, Q_m of the injected gas is estimated by;

$$Q_m = \frac{eCA_{throat}\sqrt{2\rho\Delta p}}{\sqrt{1-\beta^4}} \quad \text{(E-3)}$$

where,

e, the gas expansibility factor.

C, the gas discharge coefficient.

A_{throat}, throat area of the injection tube, m^2.

Δp, the differential pressure, Pa.

β, the ratio of the diameter of the injection tube, d to the diameter of the test pipe, D. That is, $\beta = d/D$

The gas expansibility factor, e is calculated by;

$$e = 1 - (0.41 + 0.35\beta^4)\frac{\Delta p}{KP} \quad \text{(E-4)}$$

The gas density at operating conditions is estimated by;

$$\rho = \frac{MWP}{R_c T} \quad \text{(E-5)}$$

and,

$MW = 0.028\ kg/mol$

Note that,

A_{throat}, throat area of the injection tube is estimated by;

$$A_{throat} = \frac{\pi}{4}d^2 \quad \text{(E-6)}$$

The differential pressure, Δp is calculated by;

$$\Delta p = mP \quad \text{(E-7)}$$